Chinese Journal of Chemical Engineering 25 (2017) 1524–1532

Contents lists available at ScienceDirect

Chinese Journal of Chemical Engineering

journal homepage: www.elsevier.com/locate/CJChE

Energy, Resources and Environmental Technology

Microencapsulation of stearic acid with polymethylmethacrylate using iron (III) chloride as photo-initiator for thermal energy storage☆

Ting Zhang [1], Minmin Chen [1], Yu Zhang [1], Yi Wang [1,2,*]

[1] College of Petrochemical Technology, Lanzhou University of Technology, Lanzhou 730050, China
[2] State Key Laboratory of Advanced Processing and Recycling of Nonferrous Metals, Lanzhou University of Technology, Lanzhou 730050, China

ARTICLE INFO

Article history:
Received 22 November 2016
Received in revised form 19 April 2017
Accepted 21 April 2017
Available online 1 May 2017

Keywords:
Thermal energy storage
Phase change material
Microencapsulation
Thermodynamic properties
Synthesis
Photochemistry

ABSTRACT

Aiming to identify the validity of fabricating microencapsulated phase change material (PCM) with polymethylmethacrylate (PMMA) by ultraviolet curing emulsion polymerization method using iron (III) chloride as photoinitiator, SA/PMMA microcapsules were prepared and various techniques were employed to determine the ignition mechanism, structural characteristics and thermal properties of the composite. The results shown that the microcapsules containing SA with maximum percentage of 52.20 wt% formed by radical mechanism and only physical interactions existed in the components both in the prepared process and subsequent use. The phase change temperatures and latent heats of the microencapsulated SA were measured as 55.3 °C and 102.1 $J \cdot g^{-1}$ for melting, and 48.8 °C and 102.8 $J \cdot g^{-1}$ for freezing, respectively. Thermal gravimetric analysis revealed that SA/PMMA has good thermal durability in working temperature range. The results of accelerated thermal cycling test are all shown that the SA/PMMA have excellent thermal reliability and chemical stability although they were subjected 1000 melting/freezing cycles. In summary, the comparable thermal storage ability and good thermal reliability facilitated SA/PMMA to be considered as a viable candidate for thermal energy storage. The successful fabrication of SA/PMMA capsules indicates that ferric chloride is a prominent candidate for synthesizing PMMA containing PCM composite.

1. Introduction

Development and utilization of renewable energy sources have received increasing attention in recent years due to the exhaustion of conventional fossil fuels, increasing of combustion-generated pollutants and the continuing rise in energy prices. The direct solar radiation is considered to be the most promising cornerstone for solving the global energy crisis worsening gradually in view of its well-known features. However, the large-scale utilization of this form of energy confronted with a lot of technical and economic problems. Thermal energy storage (TES) remains among the ranks of these problems, especially when talking about long-term storage, due to the intermittent and instability characteristics of solar energy. A suitable TES forms not only reduces the mismatch between supply and demand, decreases the excess energy wasted, but also improves the performance and reliability of energy systems. Unfortunately, energy stored in suitable forms which can be conveniently converted into the required style is a present day challenge to the technologists [1].

The basic types of thermal energy storage techniques can be classified as sensible heat storage, latent heat storage and thermo-chemical energy storage [2]. Among these ways of thermal energy storage, latent heat thermal energy storage (LHTES) using phase change materials (PCMs) as storage media is a particularly attractive technique because the advantage of high heat-storage efficiency, temperature stability, and easy control in the phase change process [1,3]. What's more, LHTES system requires smaller weight or volume of material for given amount of energy when compared with the conventional sensible heat energy storage system due to the high storage density. The unique features makes LHTES and PCMs widely applied in many fields, such as water- and air-heating systems, solar greenhouses, solar cookers, heat transfer and building materials [1–4].

Various chemical substances (more than 160000 [5]) have been investigated as PCMs for LHTES applications, which are usually classified into two major categories: inorganic and organic compounds [1,6]. Although most inorganic PCMs have the advantages of high volumetric latent heat storage, relatively high thermal conductivity, cheaper and readily available, they often suffer from serious supercooling and phase segregation during the solidification process. Compared with inorganic PCMs, organic PCMs avoid the above disadvantages inherent

☆ Supported by the National Natural Science Foundation of China (51562023), the Natural Science Foundation of Gansu Provence (145RJZA185) and the National science and technology support project (2014BAA01B01).
* Corresponding author.
E-mail addresses: wangyi@lut.cn, haoyunwangyi1977@163.com (Y. Wang).

http://dx.doi.org/10.1016/j.cjche.2017.04.013
1004-9541/

in inorganic compounds and possess good stability and relatively high latent heat [6,7]. Among the investigated organic PCMs, stearic acid (SA), a kind of linear chain fatty acid, is the mostly employed PCM for practical LHTES applications [8–10]. Due to the fact that different PCMs have different characteristics, undesirable and desirable properties, an evaluation system of three levels and six attributes based on the VIKOR method was established in previous study [11] to sort out the optimal PCM comprehensively. The results also shown that SA is the optimal PCM among the candidates for low-temperature thermal energy storage because of its desirable features of high heat energy heat capacity, negligible super-cooling, smaller volume change and good thermo-chemical stability after long-term utility period. Another important advantage of this fatty acid is it can be obtained from vegetable and animal oils which provide a continuous supply [6]. However, employing SA in traditional manner has several defects, *i.e.* low thermal conductivity and leakage during phase change process which cause the necessity of using special stored devices and additional heat exchange surface, increasing the associated cost and thermal resistant between the PCM and the environment [12]. In order to overcome these drawbacks, many techniques are investigated and microencapsulation is considered to be probably the best solution [13,14].

Microencapsulation is a process of coating individual particles or droplets with a continuous film to produce capsules in a micrometer to millimeter in size, known as microcapsule. The ultimate aim for microencapsulated PCMs (MEPCMs) is to achieve nanosize particles and high ratio of the surface area to volume which is expected to overcome the low thermal conductivity problem and provide an inert shell which protects sensitive PCMs from environment or makes PCMs easier and/or safer to handle [6,13,15]. In addition, the MEPCMs can be easily incorporated into many matrixes [13]. MEPCMs are composed of two main parts: PCM as core and polymer or inorganic materials as shell. Therefore, wall material selection also is the crucial procedure in fabricating capsules and an appropriate shell may regulate the properties of the microcapsules, such as morphologies, heat capacities and thermal stabilities [1,6]. Up to now, various polymers or inorganic materials have been extensively used for the encapsulation of PCM, such as polyurea [16], gelatin/acacia [14], silica [17] and polymethyl methacrylate (PMMA) [18–20]. The current finding on MEPCMs indicated that methyl methacrylate (MMA) as the monomer for shell had attracted more and more attention [21,22]. PMMA is a thermoplastic, transparent and commercially available acrylic resin with the attractive properties of non-toxic, easy handling and processing, relative chemical resistance and high impact strength, which makes it to be a promising polymer for preparing microcapsules containing PCMs in TES applications [23]. Beyond these, slightly hydrophilic properties of the monomer also give them higher solubility and reactivity in water, which finally improve the efficiency of PCM encapsulation [13].

Several physical and chemical methods are used for producing MEPCMs with PMMA shell such as the suspension copolymerization-solvent volatile method [24], emulsion polymerization technique [18,23,25,26], solution casting method [19], self-polymerization method [27], in-situ polymerization method [28], suspension polymerization [21] and irradiation-initiated emulsion polymerization method [20,29,30]. There are many signs suggesting that a well-designed photo-polymerization might provide a number of features compared to traditional thermal-activated process, such as higher reaction rate because of the rapid and energy efficient initiation, easily spatial and temporal operation due to the reaction rate and molecular weight of the polymer could be tuned by varying light intensity or irradiation time, minor risk of colloidal destabilization as the reaction is carried out at ambient temperature [31]. These suggest that light-induced polymerization might be a substantially improved technology for fabricating PMMA based MEPCMs and this feasibility has been identified by S. Ma et al. [20] and our group [29,30]. But beyond these, to the best of our knowledge, studies focused on MEPCMs using photopolymerized method are still rare. On the other hand, the used photoinitiators, a very important and necessary component in UV irradiation induced polymerization system, are all traditional radical and cationic initiators such as Photocure®1173 (2-Hydroxy-4′-(2-hydroxyethoxy)-2-methylpropiophenone), Photocure®2959 (1-[4-(2-Hydroxyethoxy)-phenyl]-2-hydroxy-2-methyl-1-propan-1-one) and *etc.* [19,20,29–32]. These widely used organic initiators have enviable price although it has good performance of ignition, *e.g.*, the cost of Photocure®2959 would be 150 to 200 times as much than traditional inorganic initiators according to the announced price on the Website of Sigma-Aldrich Company. Therefore, many attempts have been made to initiate the polymerization of vinyl monomers using inorganic photoinitiator [33,34] and the results indicate that iron complexes (like $[Fe(bipyridine)_3]^{3+}$ and $[Fe(C_2O_4)_3]^{3-}$) may be the most promising one in the presence of amines [34–36]. However, as far as we know, there are few works that have been done on the UV-induced emulsion photopolymerization of MMA using Fe(III) as initiator, let alone preparing MEPCMs. Therefore, it is worthwhile to identify the feasibility of fabricating MEPCMs by ultraviolet irradiation-initiated method using iron (III) chloride as initiator and investigate the difference of thermo-chemical property. It is not difficult to understand that the studies like this are expected to develop a new manufacturing approach of the MEPCMs, which is one of the essential goals of green chemistry.

On the basis of this understanding, together with the greater importance of TES, SA/PMMA MEPCMs were fabricated *via* UV initiated emulsion polymerization method using iron (III) chloride as initiator in current work aiming to develop an excellent composite PCM, evaluate the differences of performance and reduce the preparation cost. And on this basis, Fourier transformation infrared spectroscope (FT-IR), scanning electronic microscope (SEM), differential scanning calorimetry (DSC), thermogravimetric analyzer (TGA), thermal performance test and accelerated thermal cycling test (ATC) were employed to investigate the chemical characteristics, thermal properties and reliability of composite, respectively.

2. Experimental

2.1. Materials

SA (Commercial Grade, Beijing Chemical Co. Ltd., China) and MMA (Analytical Reagent, Aladdin company, China) were used as PCM and shell-forming monomer, respectively. The monomer was washed by 5% NaOH solution (V_{MMA}:V_{NaOH} = 5:1) and deionized water in a separatory funnel for several times to remove the polymerization inhibitor and then double distilled under reduced pressure prior to use. Ethyleneglycol dimethacrylate (EDMA, Shanghai Hechuang Chemical Co. Ltd.) was used as crosslinking agent and cetyl trimethyl ammonium bromide (CTAB, Shanghai Zhongqin Chemical Reagent Company) was served as emulsifier. Hexahydrated ferric chloride (Analytical Reagent) supplied by Tianjin Chemical Reagent Factory and used as the source of iron (III) complexes. The other photosensitive reagent, Photocure®1173, Photocure®2959 and BDK (2, 2-dimethoxy-2-phenylacetophenone) were bought from Sigma-Aldrich Company. In addition, deionized water was self-made by our laboratory.

2.2. Preparation of SA/PMMA microcapsules

UV photo-initiated emulsion polymerization method was employed to prepare the SA/PMMA capsules. Typical synthetic process is as follows: 40 ml deionized water, a certain amount of SA and 0.2 g CTAB were poured into 250 ml beaker and the pH value of the aqueous solution was adjusted to 2.0 by hydrochloric acid. Then, the given mass of $FeCl_3 \cdot 6H_2O$ was added and the mixture was heated above melting point of SA under magnetic stirring until SA melted completely. Afterward, the heating was stopped and 5.0 g refined monomers were added. The above solution containing all of materials was firstly dispersed vigorously by a homogenizer (ultra-turrax high speed homogenizer, Ika T50 basic, Germany) at 10000 $r \cdot min^{-1}$ about 5 min, and then continued to disperse with an ultrasonication cleaner (Kunshan, KQ3200DE,

China) for another 10 min at the room temperature to form an emulsion. The Oil/Water emulsions were poured into a tailored low columned quartz container and irradiated by UV light of 2500 W without stirring for desired time. Finally, in order to remove the unreacted reactants and uncoated SA, the resultant was filtered and washed with warm distilled water (approx. 70 °C) and ethyl alcohol several times till the filtrate becomes clear. The residue was collected, dried under vacuum at 50 °C for 24 h and the incompact white powers were obtained and recorded as SA/PMMA.

In order to discuss the efficiency of the light initiator and comparative study, the controlled experiments were also carried out and the conversion ratio (CRO) of MMA was investigated in the same way only without SA added. In the process of reaction, 2 ml reactants were collected at regular intervals and 0.05 ml hydroquinone solution (5 wt%), 25 ml methanol was added to stop the reaction and precipitate the products. The residue was collected and dried at 105 °C for 24 h and the CRO is calculated according to the Eq. (1), where w_1 and w_2 are the mass in g of products and reactants in the solution, respectively.

$$\mathrm{CRO} = w_1/w_2 \times 100\% \quad (1)$$

2.3. Characterization of SA/PMMA microcapsules

Thermal energy storage properties of SA and SA/PMMA microcapsules were determined by DSC (NETZSCH DSC200F3, Netzsch Ltd. Germany) at a heating rate of 5 °C per minute and temperature range from 0 °C to 100 °C in a purified nitrogen atmosphere. The surface morphology and microstructure were observed by using a SEM (JSM-6701, JEOL Ltd., Japan). Before the investigation, all specimens were sputter-coated with gold in vacuum conditions to avoid charge accumulations and all analyses were performed at room temperature at acceleration voltage of 20 kV. The spectroscopic analyses of raw materials and the as-prepared samples were performed on a KBr disk in the range of 4000–400 cm^{-1} by using a FT-IR (Nicolet Nexus 670, USA) instrument. The thermal stability was determined by means of thermogravimetry on a TGA (NETZSCH STA-449F3, Netzsch Ltd. Germany). The analyses were carried out under N_2 atmosphere at a flow rate of 20 ml·min^{-1} and a linear heating rate of 10 °C·min^{-1} from room temperature to 800 °C. The particle size distribution (PSD) of the resin and capsules were determined with a laser diffraction particle size analyzer (MASTERSIZER 3000, Malvern Instruments Ltd., UK) in a diluted dispersion of the particles in water. The molecular weight and its distribution of PMMA resin was investigated by the way of gel permeation chromatography (WATERS 1515, Waters Corp. USA) at room temperature using tetrahydrofuran as solvent and eluent. In order to determine thermal reliability of SA/PMMA, ATC test (1000 melting/freezing processes) and thermal energy storage/retrieval performance experiment were also conducted using a home-made device which described in Ref. [9,29,30]. After repeated numbers of thermal cycling, DSC analysis, FT-IR spectrophotometer, morphology and TGA were employed to evaluate the thermal reliability of the samples.

3. Results and Discussion

3.1. Feasibility of fabricating SA/PMMA employing iron (III) chloride as initiator

The effect of photo-initiator on the conversion of MMA photopolymerization which determined by gravimetry is described in Fig. 1. As can been seen, no matter which kind of photoinitiator was used, the conversion percentage increased with the extension of radiating time and the maximum yields were achieved in 30 min of irradiation. This result is sharp against several hours traditionally with a heat-activated polymerization process in a dispersed medium to reach the limiting conversions [31]. The higher reaction rate is due to the turbid dispersed medium could be even beneficial to the photochemical

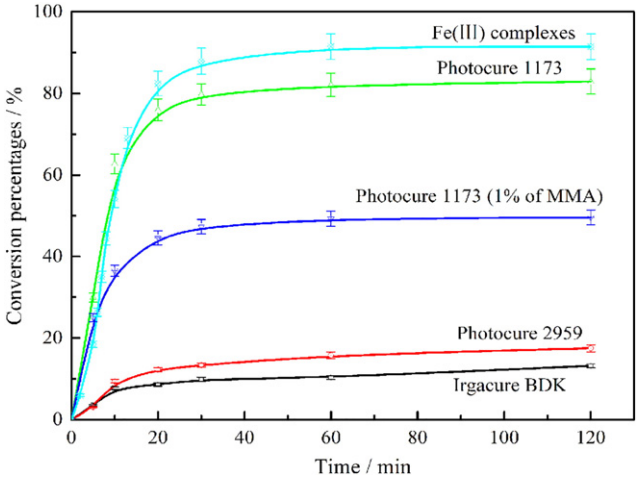

Fig. 1. Conversion–time curves for PMMA synthesized with different initiators.

process since light is scattered many times, which might increase the quantum yield of the photoinitiator [35]. However, enormous difference of accomplished conversion existed in different initiator and the ferric chloride has the biggest ignitor efficiency under the experimental conditions. The reason of this difference may lie in two aspects, the initiated pathways and the UV absorption properties of the initiator. The radical species generated in the aqueous phase and then penetrated into the monomer droplets to trigger the polymerization for the water-soluble photo-initiator, while it readily incorporated in monomer droplets before UV irradiation for the oil-soluble photo-initiator. According to the results of thermal induced emulsion polymerization, more resultants will be received when particles formed by other processes using water-soluble initiator than droplet nucleation [35]. On the other hand, as we all know, $[Fe^{(III)}(H_2O)_6]^{3+}$ is the dominant species at low pH (<2.5) [37]. The main absorption bands of iron salt in water ($[Fe^{(III)}(H_2O)_6]^{3+}$) are 220 and 300 nm [31]. So, the iron (III) chloride is the optimum photoinitiator in our irradiation conditions because the maximum absorption for Photocure®1173 is about 245 nm, 280 nm and 331 nm and Photocure®2959 is around 276 nm and 331 nm, respectively.

The effect of ferric chloride usage amount on the conversion of monomer is shown in Fig. 2. It is clear that the conversion percentages of MMA increased firstly, then slightly decreased and the CRO received maximum value when mass ratio of ferric chloride and MMA is 0.7 wt%. This is contributed to the changes of polymerization rate which could be initiated with different efficiency by the excitation of iron complexes with different ligands (usually is solvent). The hexaaquo complexes, in present study is

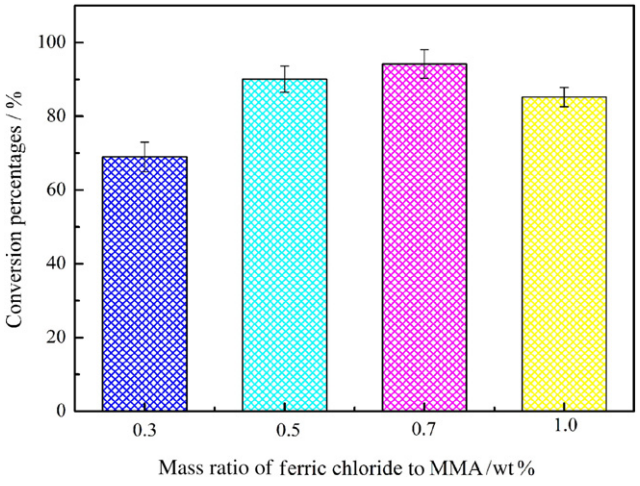

Fig. 2. Effect of initiator consumption of on the conversion of MMA.

$[Fe^{(III)}(MMA)_6]^{3+}$ and $[Fe^{(III)}(H_2O)_6]^{3+}$, have typical Ligand-to-Metal Charge Transfer (LMCT) absorption bands which extend into the visible region [34]. When the ligands are water molecules, the photo polymerization of MMA will proceed *via* a radical mechanism [34]. When the external power was given, the central iron ion in the excited complexes will accept an electron from one of the ligands, resulting in the formation of Fe(II) ion and a free radical (OH·) [31,35,37] which then initiated the polymerization occurring by the well-known addition mechanism. The concise mechanism is represented in Fig. 3. In the case of high mass ratio of Fe(III) with MMA, partially Fe(III) combined with MMA and the mechanism proceed via the direct oxidation of the monomer to yield an initiating cation radical, which described in Ref [31] in detail. Due to the lower radical production efficiency of the $[Fe^{(III)}(MMA)_6]^{3+}$ complex, the conversion is gone down at the limited period time.

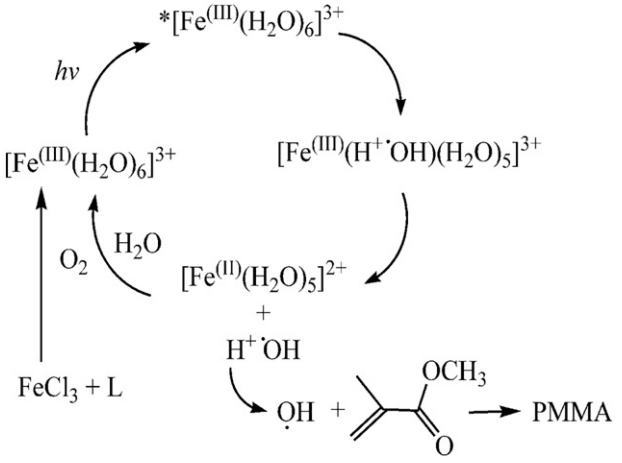

Fig. 3. Mechanism of free radical ejected in the presence of Fe(III) complexes at the aqueous solution.

3.2. Determination of optimum core-shell mass ratio

For microencapsulated phase change material, PCM is employed as the core to store thermal energy during the phase transition and the polymer, inorganic material or organic–inorganic hybrid material is used as shell to encapsulate the PCMs, which in turn isolates them from the external environment [38]. Therefore, the higher content of PCMs in microencapsulated PCMs will result in the higher heat storage capacity and excellent viability as well as the less usage of the material due to the shell has no contribution for latent thermal energy storage capacity [39]. However, the excessive PCM located in the emulsion will result in incomplete encapsulation or thin wall, which ends the result in leakage. Therefore, a series of SA/PMMA capsules with an increased core-shell mass ratio of 45%, 50%, 53% and 56% were prepared to identify the optimal composition. In order to ensure that the as-prepared samples are all form-stable and no leakage, all of the pre-drying specimens which were fabricated in different recipes were placed on the filter papers and heated at 70 °C for 2 h in an oven and the leakage was determined by gravimetric analysis and visual surface inspection. Only the samples which have a mass change less than 1% before and after heating are defined as form-stabilized MEPCMs. Partly photograph images of leakage experiment are shown in Fig. 4. As seen from the photographs, the as-prepared PCMs are all powders with slightly yellowish appearance due to the usage of iron (III) chloride. The sample stack started to crack firstly with the increase of PCM percentage, and eventually emerged leakage along with the propagation of crack when SA mass fraction is larger than 53%. On the basis of the above experimental facts, it can be concluded that 53% is the optimal SA mass fraction to fabricate SA/PMMA MEPCMs against the PCM seepage problem.

3.3. Morphology and chemical characteristics of SA/PMMA microcapsules

Surface roughness and particle size play a vital role in thermal degradation, heat transfer rate, storage and transportation properties in their fruitful use [1,38,40]. SEM observations of PMMA (a) and SA/PMMA (b) and their particle size distribution graph (c) have been given in Fig. 5. It can easily be seen in Fig. 5(a) and (b) that most of PMMA and SA/PMMA have exactly spherical structure with smooth and compact profiles, but somewhat ellipsoid in shape. The similar appearance of PMMA and its composite, as differentiated from SA, together with the results of leakage experiment, indicates that SA was successfully encapsulated. The obvious distinction lies in the different sizes of the resin and its composites. From Fig. 5(c), the SA/PMMA capsules have larger average diameter (approx. 290 nm) and broaden distribution than neat resin (about 150 nm). The mean diameter in PSD curves are all larger than that observed in SEM micrograph due to

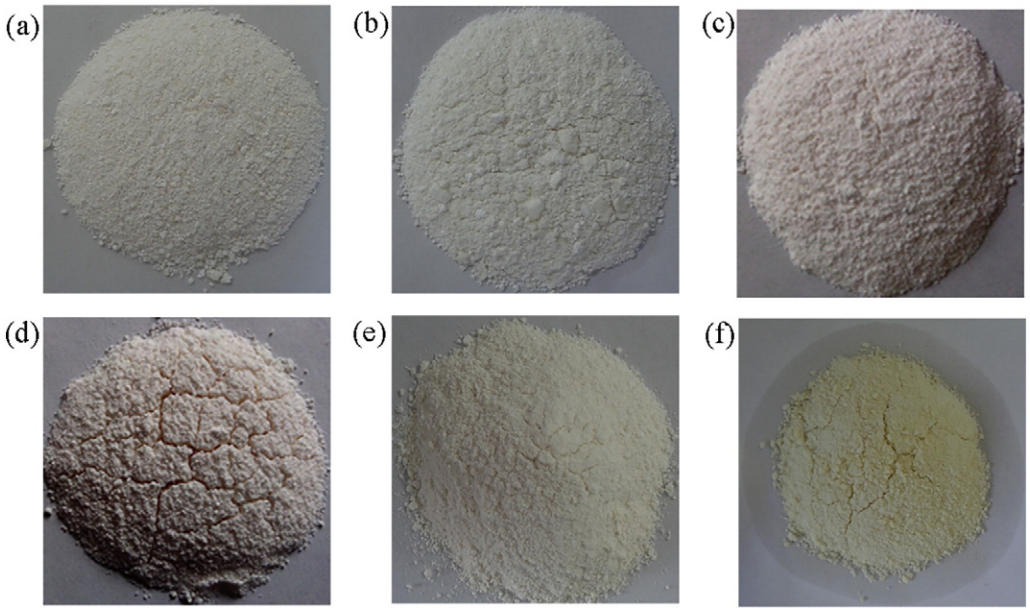

Fig. 4. Photograph images of SA/PMMA before (a, c, e) and after (b, d, f) leakage experiment fabricated with the SA percentage of 50% (a, b), 53% (c, d) and 56% (e, f).

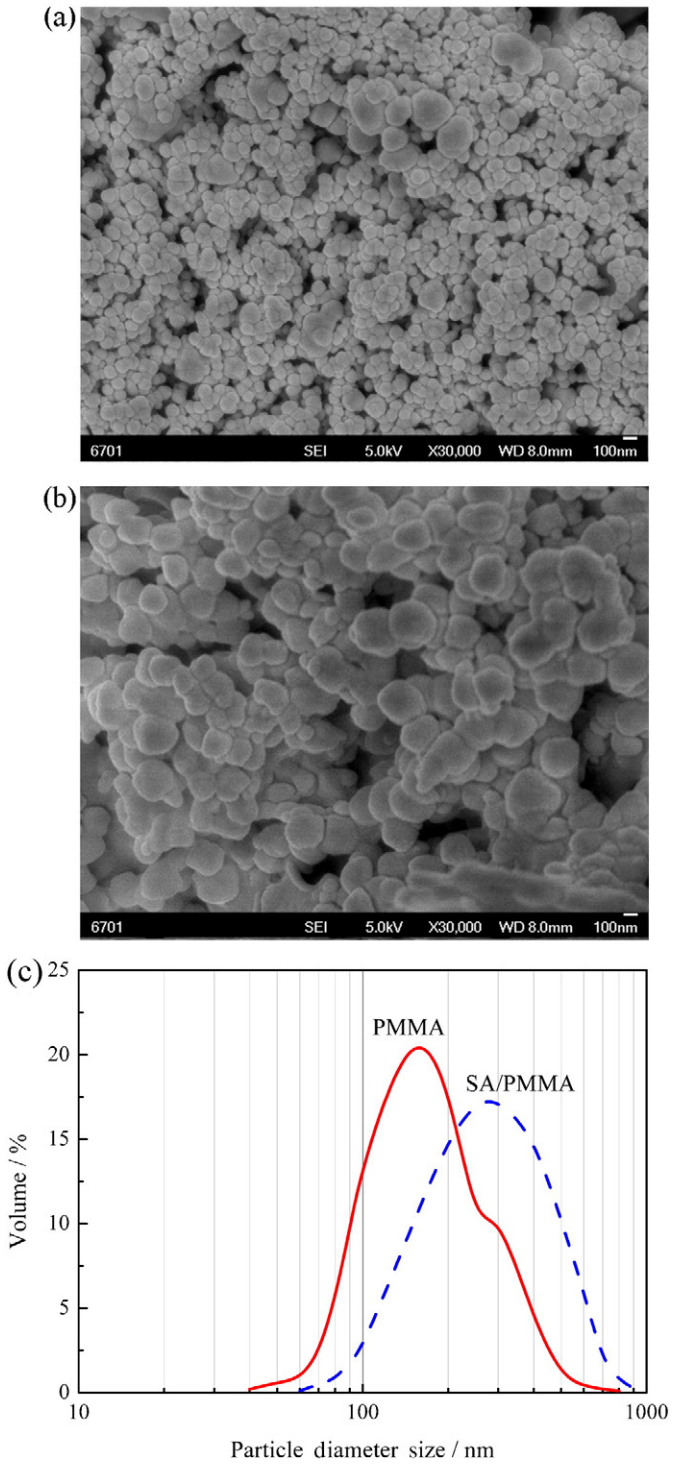

Fig. 5. SEM micrographs (a, b) and particle size distribution diagram (c) of PMMA and SA/PMMA.

adhere and aggregate of the particles. The dimension of encapsulated PCM is mainly controlled by the size of emulsified core material which is related directly to the inputted energy, stability, characteristic viscosity and interfacial tension of the emulsion [40,41], although the thickness of shell can be changed largely by the shell structure [30]. In this study, the oil-in-water emulsion which can be stable up to 30 min was formed firstly due to the hydrophobic functional groups of C—H and similar density of the oil phase [42]. Vigorous stirring is benefit for produce smaller droplets and emulsions with a narrow droplet size distribution. As reported in water-in-oil emulsion previously, the smaller droplet size results in higher viscosity. In order to reduce the viscosity of the emulsion, the fine droplets come closer and coalesce which eventually result in the growing up of the droplets. Due to the higher concentration of dispersed phase (oil phase), coalescence would be faster in SA/PMMA preparation process and hence the decrease in the viscosity might broaden the droplet size distribution and increase the particle size [40]. Moreover, the feature of molecular self-assembly makes backbone chains in fine droplet reassembling, and finally the microstructure of monomer exposed on the droplets surface is formed because of the shorter hydrophobic segment and relatively good water-solubility of MMA. This orientation of molecular groups eventually results in the formation of capsules with core/shell structure under the UV initiated polymerization.

The interactions between SA and PMMA were investigated by FT-IR spectroscopy and the typical spectra are shown in Fig. 6. In the spectra of SA, the peaks at 2919 cm^{-1}, 2849 cm^{-1} represent the symmetric and asymmetric stretching vibration of aliphatic C—H group, respectively, which usually overlaps with the stretching vibration of O—H group. The absorption peak at 1700 cm^{-1} is assigned to the C═O group stretching vibration. The peak at 1471 cm^{-1} corresponds to the bending vibration of —CH_2, 1301 cm^{-1} represents the in-plane bending vibration of C—H, 940 cm^{-1} and 720 cm^{-1} corresponding to the out-plane bending vibration and rocking vibration of the functional group of C—H, which are all characteristic for aliphatic chain of SA. The FT-IR spectra of PMMA exhibits two main absorption peaks, the most intensive absorption band at 1730 cm^{-1} represents stretching vibration of carbonyl group and the peak around 1147 cm^{-1} belongs to the stretching vibration of C—O [18,20,25]. When take the spectra of SA, PMMA and SA/PMMA into comprehensive consideration, it is clearly seen that each of the characteristic peaks belonging to SA and PMMA preserve itself. Moreover, no significant new peak is observed in the infrared spectrum of the capsules which confirm the good compatibility and just a physical interaction between SA and PMMA. These results coincided with the conclusions of other researches about PMMA containing paraffin [20], *n*-docosane [26], *n*-octacosane [25], fatty acid eutectic [18] and SA [9,30]. On the other hand, the evidence of successful encapsulation is still existed in the spectrum of SA/PMMA. The slightly red-shifted position of the carbanyl group which is sensitive to the physical attractions and the decreased strength of the characteristic peaks of SA suggest that SA is well coated and there are physical interactions between hydrogen atom of hydroxyl group of fatty acid and oxygen atom of carbonyl group of PMMA [39].

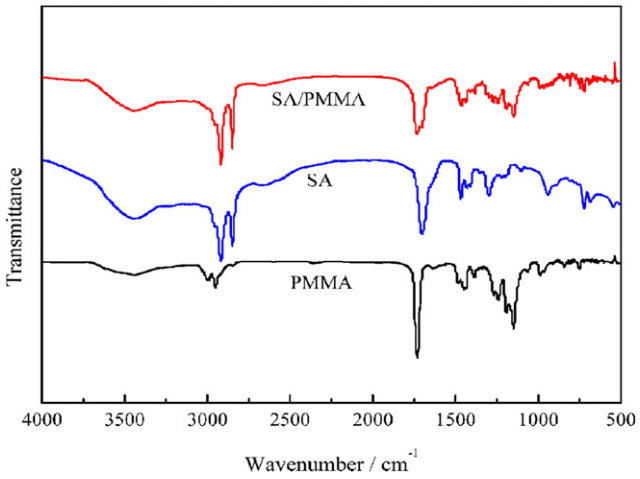

Fig. 6. FT-IR spectra of SA, PMMA, SA/PMMA capsules.

3.4. Thermal properties of SA/PMMA microcapsules

Thermal energy storage properties of the raw material and SA/PMMA were investigated by DSC analysis and the results are illustrated in Fig. 7. As can be seen in Fig. 7, each DSC curve of the samples

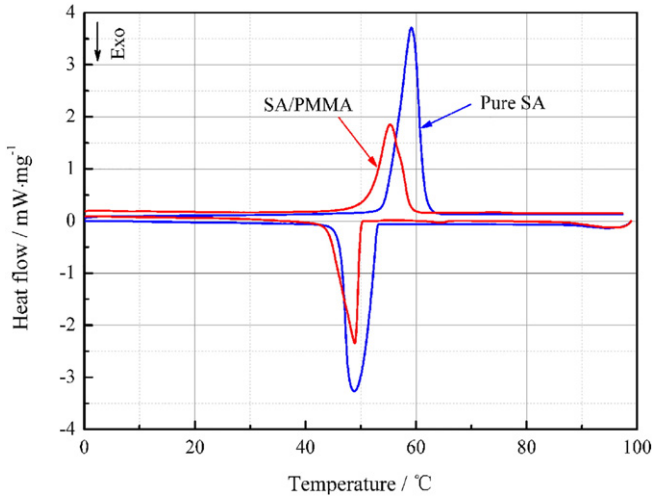

Fig. 7. DSC thermogram of SA and SA/PMMA.

possesses two sharp phase change peaks which represent the solid–liquid or liquid–solid phase transition of SA and its composite. The extrapolated onset temperature (T_{om} and T_{oc}), peak temperature (T_{pm} and T_{pc}) and extrapolated end temperature (T_{em} and T_{ec}) of SA are determined to be 55.0 °C, 59.2 °C and 61.5 °C for melting (m) and 46.5 °C, 48.8 °C and 52.9 °C for crystallization (c), while the corresponding temperature of SA/PMMA is evaluated to be 51.8 °C, 55.3 °C, 59.0 °C and 49.9 °C, 48.8 °C, 44.1 °C, respectively. Both DSC curves exhibit identical shapes also indicating that there is no chemical reaction between the core and the shell material and the thermal energy storage property of MEPCMs comes from the core. However, SA/PMMA has lower melting temperature, slightly higher crystallizing temperature and smaller super-cooling degree than SA. Due to the similar volume expansion coefficient of SA and PMMA [27], it seems that the deviation of phase change temperature is not caused by the additional stress which came from the change of fatty acid volume restricted by the walls [43]. However, it is in agreement with the conclusion of PCMs/porpous media composite, that is, a weakly attractive interaction between fluid molecules and surface of matrix will result a depressed melting phase change temperature [44]. We believe that the above proposal is also satisfied with the SA/PMMA capsules. The beneficial attractive interaction in SA/PMMA is attributed to the damage of carbonyl acid dimeric structure induced by the interaction between SA and PMMA [27,30]. In addition, the decreased super-cooling degree of the capsules seems to announce that the validity of encapsulation could slightly decrease the supercooling degree of the PCMs [25].

On the other hand, the latent heat ($\triangle H$) obtained as the area under the peaks of the phase transition for melting ($\triangle H_m$) and crystallizing process ($\triangle H_c$) were found to be 195.6 $J \cdot g^{-1}$ and 197.4 $J \cdot g^{-1}$ for SA and 102.1 $J \cdot g^{-1}$ and 102.8 $J \cdot g^{-1}$ for SA/PMMA capsules, respectively. The mass content of SA in capsules is further calculated as 52.20% through dividing the measured enthalpy of microcapsule by the value of SA based on the assumption that microencapsulation does not affect the enthalpy of core materials. The calculated percentage of SA is very close to the fabricated mass fraction (53%) indicating that all of SA is encapsulated successfully. Moreover, the comparison of thermal energy storage properties of the as-prepared SA/PMMA with that of the different composite PCMs using PMMA as wall material available in literatures is given in Table 1. It can be easily observed that the latent heat of SA/PMMA capsules prepared in the present study is higher than most of composite prepared by traditional technology or UV curing method using organic initiator. The comparable thermal storage ability confirmed that iron (III) chloride is an effective and practical photoinitiator to synthesize PMMA containing PCM composite.

The other crucial issue, the resistance against thermal degradation which limited the application area of the composite PCMs, was also investigated by TGA and the results are shown in Fig. 8. As can be seen in Fig. 8, the SA degrades in one step as PMMA resin degrades in two steps, which is similar to the observation of Alkan [19]. The two degradation steps of PMMA are not easily distinguishable in TG analysis (Fig. 8(a)), but it can be clearly observed in Fig. 8(b) due to the two maximum endothermic peaks that emerged at 295 °C and 375.9 °C. For the SA/PMMA composite, the first thermal decomposition step occurs roughly at 215 °C and ends at 320 °C and the second weight loss processes within 320–430 °C. It is hard to determine the causes of the first weight change due to the fact that the initial degradation temperature of SA and PMMA is very close to each other. Thanks to the volatilization of the SA that is complete when temperature increased to 320 °C, we can safely conclude that the second degradation around 410 °C, about 40%, attributes to the decomposition of PMMA. Therefore, the rest of weight loss, which is higher than the SA content in SA/PMMA, corresponds to volatilization of the SA and other volatile species. Due to degradational temperature of SA/PMMA is higher than 200 °C, the prepared form-stable PCMs are supposed to be applied in the thermal energy storage system when working temperature is lower than 200 °C.

3.5. Thermal reliability of SA/PMMA microcapsules

The economic feasibility of LHTES system depends on the life of the thermal energy storage medium. Therefore, the comprehensive knowledge of the thermal properties and thermal reliability of a potential PCM should be verified by a thermal cycling test to assure the long term stability before usage. The surface morphology and chemical stability of SA/PMMA after 1000 ATC test is demonstrated in Fig. 9. As shown in Fig. 9(a), all of the cycled microcapsules maintain the original spherical shape. Thanks for the higher number-average molecular weight (8.16×10^4, $M_w/M_n = 2.196$) and good mechanical strength of

Table 1
Comparison of thermal properties of some composite PCMs with PMMA shell in literatures

Core material	T_{pm}/°C	T_{pc}/°C	Latent heat/$J \cdot g^{-1}$	Encapsulation ratio/%	Method	References
n-Docosane	41	40.6	54.6–48.7	28	Emulsion polymerization	[26]
n-Eicosane	35.2	34.9	84.2–78.5	35	Emulsion polymerization	[18]
n-Heptadecane	18.2	18.4	81.5,-84.7	38	Emulsion polymerization	[23]
n-Octacosane	50.6	53.2	86.4–88.5	43	Miniemulsion polymerization	[25]
Lauric(58%)-myristic acid(42%) eutectic	34.81	–	80.75	50	Self-polymerization	[27]
SA	60.4	50.6	92.1–95.9	51.8	UV irradiation (1173 as photoinitiator)	[9]
Paraffin	28	–	101	61.2	UV irradiation (2959 as photoinitiator)	[20]
Paraffin wax	55.8	50.1	106.9–112.3	66	UV irradiation (1173 as photoinitiator)	[29]
Capric(86%)-stearic acid(14%) eutectic	20.20	20.14	116.25	67	Emulsion polymerization	[45]
SA	55.3	48.8	102.1–102.8	52.2	UV irradiation (Iron(III) chloride as photoinitiator)	This study

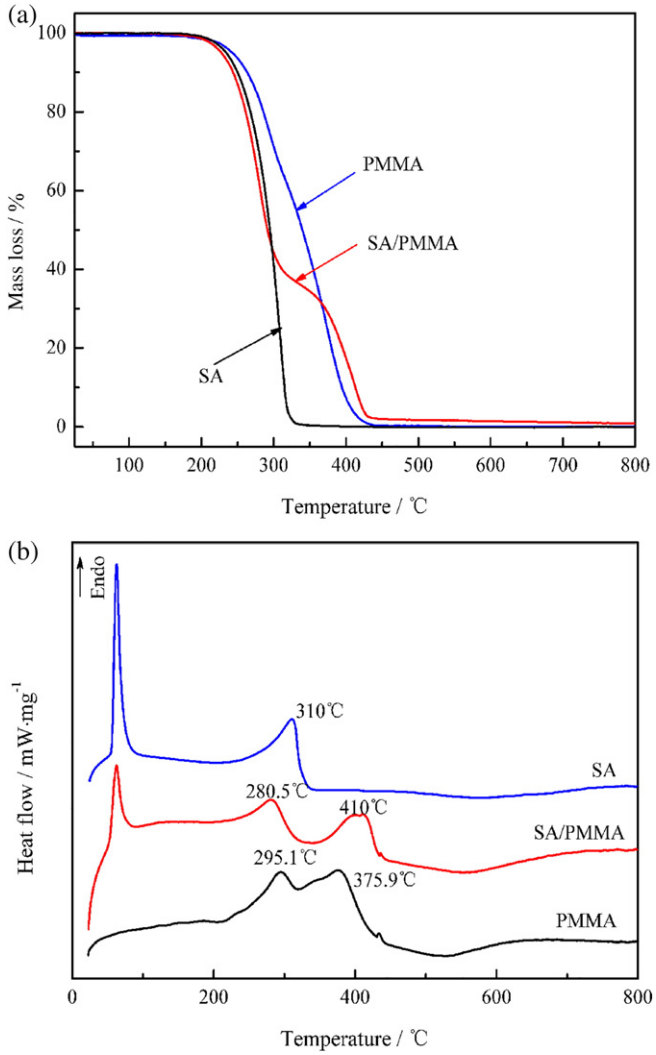

Fig. 8. TG (a) and DSC (b) analysis of SA, PMMA and SA/PMMA.

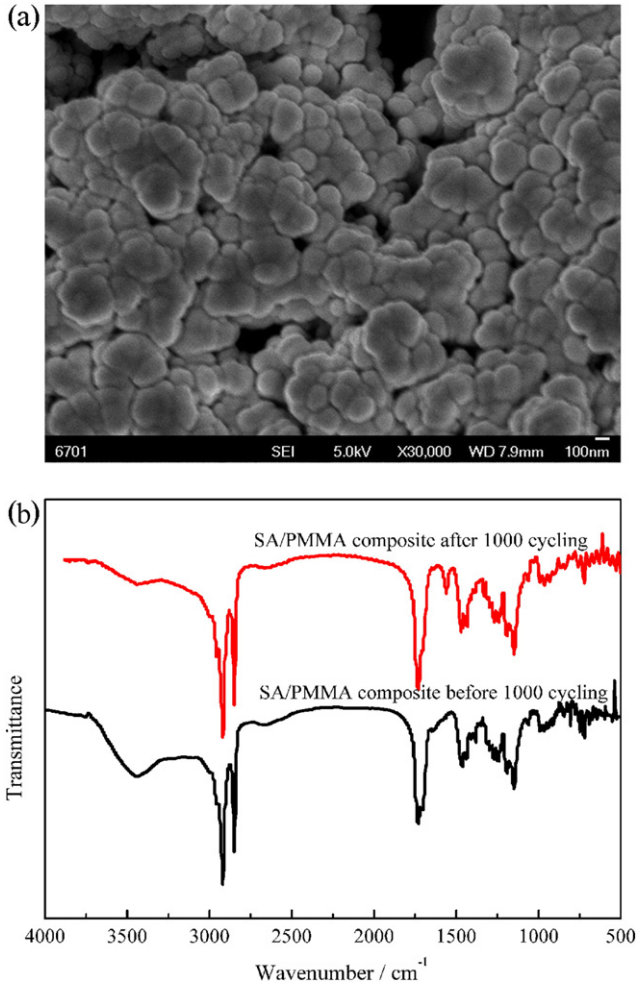

Fig. 9. SEM image (a) and FT-IR spectroscopy (b) of SA/PMMA after 1000 thermal cycles.

PMMA, the skeleton was stable against the leakage of SA from the blends and no particles prone to rupture or be deformed. Also, comparing the FT-IR spectra of SA/PMMA before and after thermal cycling in Fig. 9(b), it is clearly seen that the position of characteristic peaks did not changed after thermal cycling, indicating that the chemical structure and chemical properties of SA/PMMA and its components is stable when it endure repeated thermal cycling.

Fig. 10 illustrates the DSC curves of SA/PMMA composite before and after experiencing 1000 heating–cooling cycles and the corresponding thermographic data are shown in Table 2. The DSC curves of the capsules before and after cycling is almost overlapped and the changes of temperature or enthalpy observed in Table 2 also would be ignored. The reasonable changes of phase change temperature and enthalpy indicating that SA/PMMA has a good thermal reliability in repeated melting and freezing process.

The thermal durability of the SA/PMMA was also determined by TG analysis and the mass loss curves are displayed in Fig. 11. It is obvious that the recycled SA/PMMA has negligible weight variations compared with the pristine substance. This suggests that no chemical degradation or chemical reaction occurred during thermal cycling which is consistent with the result of FT-IR. Combine the results of SEM, FT-IR, TG and DSC of SA/PMMA endured 1000 cycling, it is worth noting that the SA/PMMA has good thermal reliability, stability and durability which are all necessary characteristics for a composite PCM with practical application.

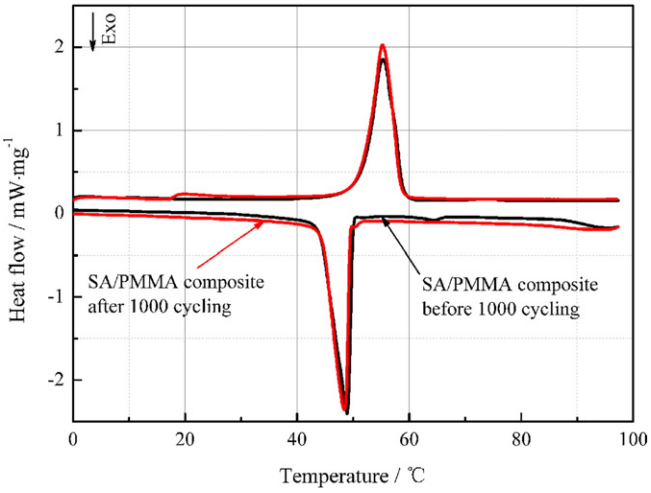

Fig. 10. DSC thermogram of SA/PMMA before and after 1000 thermal cycles.

3.6. Thermal energy storage and release performance of SA/PMMA microcapsule

The heat storage/retrieval performance and its reliability were verified by comparing the heating–cooling process of SA/PMMA before and after 1000 thermal cycling. The typical heating (a) and cooling (b) curves

Table 2
Thermal property of SA/PMMA composite before and after thermal cycling

Samples	Melting (solid–liquid phase transition)				Freezing (liquid–solid phase transition)			
	T_{om}/°C	T_{pm}/°C	T_{em}/°C	ΔH_m/J·g^{-1}	T_{oc}/°C	T_{pc}/°C	T_{ec}/°C	ΔH_c/J·g^{-1}
SA/PMMA composite	51.8	55.3	59.0	102.1	50.0	48.8	44.1	102.8
SA/PMMA after thermal cycling	51.9	55.4	58.7	101.9	49.6	48.6	44.8	102.5
Changes (absolute deviation)	0.1	0.1	−0.3	−0.3	−0.4	−0.3	0.7	−0.3

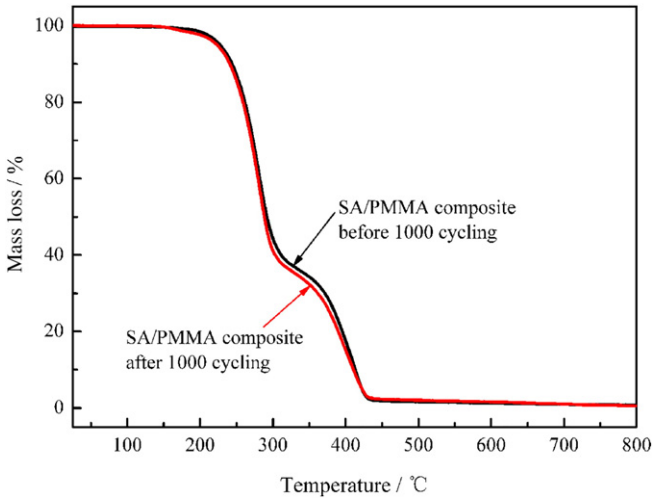

Fig. 11. TG curves of SA/PMMA before and after 1000 thermal cycles.

of the PCMs are shown in Fig. 12. As seen from Fig. 12, the temperatures of uncycled and cycled composite increased (Fig. 12 (a)) or decreased (Fig. 12 (b)) with time elapsing and the phase change then occurred. The melting and solidification time were estimated as 330 s and 550 s according to the method of constructing their outer tangent lines which are described in Ref [39]. It would be specially mentioned that the similar trend and indistinguishable changes of the temperature curves indicate that the two PCMs have similar thermal energy storage property although the cycled SA/PMMA endured 1000 cycling. This result also demonstrates that SA/PMMA not only has excellent heat storage property but also can be implemented to transfer energy in different time and space. In addition, the melting times are less than cooling times and the melting or freezing temperatures for all PCMs in Fig. 12 are lower than those from DSC because the measurement principle between heating–cooling test and DSC method are different [46].

4. Conclusions

In summary, this work aims to develop a new method to fabricate MEPCMs with PMMA shell using iron (III) chloride as initiator which is beneficial to reduce the prepared cost. For this aim, SA/PMMA capsules were synthesized *via* UV curing emulsion polymerization method and various characterization techniques were employed to investigate the conversion percentage, polymerized mechanism, morphology and thermo-chemical properties. The polymerization appeared to be completed by the radical mechanism within half an hour when ferric chloride mass is 0.7 wt% of the monomer. The SA/PMMA composite exhibits regular spherical shape with the larger particle size than its resin due to the fact that only physical interactions existed between hydrogen atom of hydroxyl group of SA and oxygen atom of carbonyl group in PMMA. The as-prepared capsules melt at temperature of 55.3 °C with latent heat of 102.1 J·g^{-1} and freeze at temperature of 48.8 °C with latent heat of 102.8 J·g^{-1}. The maximum percentage of SA was confined as 52.20 wt% without seepage of melted SA according to the determined phase change enthalpy. The results of DSC, FT-IR, TG and thermal energy storage/release analysis are all showed that SA/PMMA have good thermal reliability, thermal durability and chemical stability although they endured 1000 thermal cycling, indicating it can be used repeatedly in long term. The comparable thermal energy storage ability with similar composite prepared by thermal inducing technology and the excellent reliability not only indicate that SA/PMMA is a promising MEPCMs for TES but also verify that ferric chloride is a potential initiator for synthesizing PMMA encapsulated composite PCM.

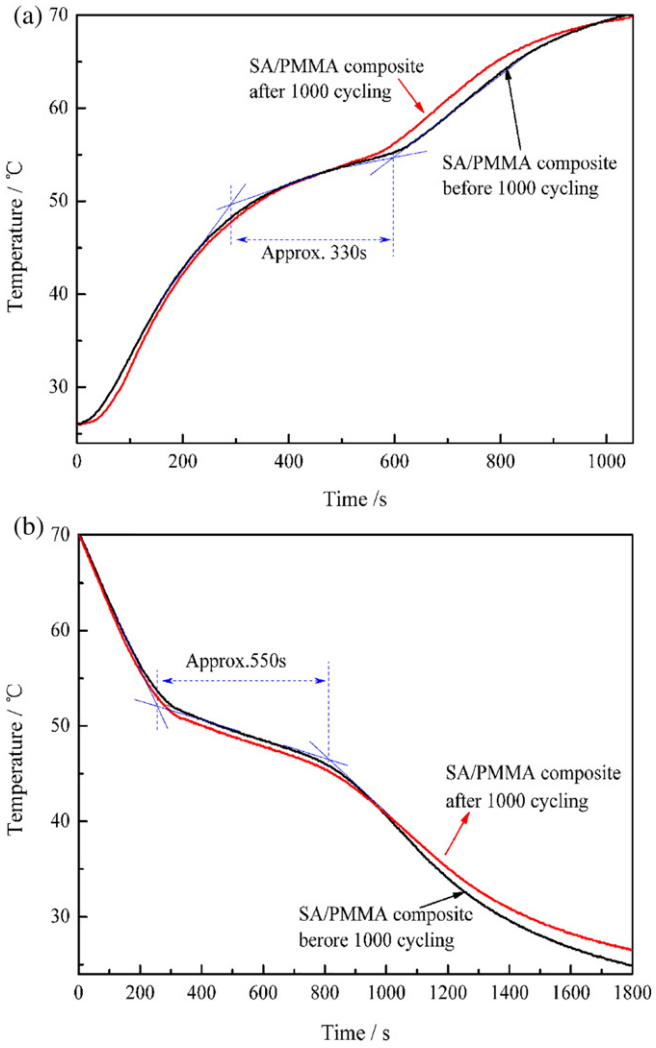

Fig. 12. Heating (a) and cooling (b) curves of SA/PMMA before and after repeated thermal cycling.

References

[1] Y.E. Miliána, A. Gutiérreza, M. Grágedaa, S. Ushak, A review on encapsulation techniques for inorganic phase change materials and the influence on their thermophysical properties, *Renew. Sust. Energ. Rev.* 73 (2017) 983–999.

[2] M. Kenisarin, K. Mahkamov, Passive thermal control in residential buildings using phase change materials, *Renew. Sust. Energ. Rev.* 55 (2016) 371–398.
[3] S.Y. Mu, J. Guo, Y.M. Gong, S. Zhang, Y. Yu, Synthesis and thermal properties of poly(styrene-co-acrylonitrile)-graft-polyethylene glycol copolymers as novel solid–solid phase change materials for thermal energy storage, *Chin. Chem. Lett.* 26 (2015) 1364–1366.
[4] X. Huang, G. Alva, Y. Jia, G. Fang, Morphological characterization and applications of phase change materials in thermal energy storage: A review, *Renew. Sust. Energ. Rev.* 72 (2017) 128–145.
[5] S. Khare, M. Dell'Amico, C. Knight, S. Mcgarry, Selection of materials for high temperature latent heat energy storage, *Sol. Energy Mater. Sol. Cells* 107 (2012) 20–27.
[6] Y. Konuklu, M. Unal, H.O. Paksoy, Microencapsulation of caprylic acid with different wall materials as phase change material for thermal energy storage, *Sol. Energy Mater. Sol. Cells* 120 (2014) 536–542.
[7] W. Su, J. Darkwa, G. Kokogiannakis, Review of solid-liquid phase change materials and their encapsulation technologies, *Renew. Sust. Energ. Rev.* 48 (2015) 373–391.
[8] A. Sharma, A. Shukla, Thermal cycle test of binary mixtures of some fatty acids as phasechange materials for building applications, *Energy Build.* 99 (2015) 196–203.
[9] Y. Wang, T. Xia, H. Feng, H. Zheng, Stearic acid/polymethylmethacrylate composite as form-stable phase change materials for latent heat thermal energy storage, *Renew. Energy* 36 (2011) 1814–1820.
[10] X. Huang, G. Alva, L. Liu, G. Fang, Preparation, characterization and thermal properties of fatty acid eutectics/bentonite/expanded graphite composites as novel form–stable thermal energy storage materials, *Sol. Energy Mater. Sol. Cells* 166 (2017) 157–166.
[11] Y. Wang, Y. Zhang, W. Yang, H. Ji, Selection of low-temperature phase-change materials for thermal energy storage based on the VIKOR method, *Energy Technol.* 3 (2015) 84–89.
[12] A. Jamekhorshid, S.M. Sadrameli, M. Farid, A review of microencapsulation methods of phase change materials (PCMs) as a thermal energy storage (TES) medium, *Renew. Sust. Energ. Rev.* 31 (2014) 531–542.
[13] K. Tumirah, M.Z. Hussein, Z. Zulkarnain, R. Rafeadah, Nano-encapsulated organic phase change material based on copolymer nanocomposites for thermal energy storage, *Energy* 66 (2014) 881–890.
[14] L. Bayés-García, L. Ventolà, R. Cordobilla, R. Benages, T. Calvet, M.A. Cuevas-Diarte, Phase change materials (PCM) microcapsules with different shell compositions: Preparation, characterization and thermal stability, *Sol. Energy Mater. Sol. Cells* 94 (2010) 1235–1240.
[15] T. Wang, S. Wang, W. Wu, Experimental study on effective thermal conductivity of microcapsules based phase change composites, *Int. J. Heat Mass Transf.* 109 (2017) 930–937.
[16] Y.H. Ma, X.D. Chu, G.Y. Tang, Y. Yao, The effect of different soft segments on the formation and properties of binary core microencapsulated phase change materials with polyurea/polyurethane double shell, *J. Colloid Interface Sci.* 392 (2013) 407–414.
[17] J.R. Li, L.H. He, T.Z. Liu, X.J. Cao, H.Z. Zhu, Preparation and characterization of PEG/SiO_2 composites as shape-stabilized phase change materials for thermal energy storage, *Sol. Energy Mater. Sol. Cells* 118 (2013) 48–53.
[18] C. Alkan, A. Sarı, A. Karaipekli, Preparation, thermal properties and thermal reliability of microencapsulated n-eicosane as novel phase change material for thermal energy storage, *Energy Convers. Manag.* 52 (2011) 687–692.
[19] C. Alkan, A. Sari, Fatty acid/poly (methyl methacrylate) (PMMA) blends as form-stable phase change materials for latent heat thermal energy storage, *Sol. Energy* 82 (2008) 118–124.
[20] S. Ma, G. Song, W. Li, P. Fan, G. Tang, UV irradiation-initiated MMA polymerization to prepare microcapsules containing phase change paraffin, *Sol. Energy Mater. Sol. Cells* 94 (2010) 1643–1647.
[21] R. Al-Shannaqetal, M. Farid, S. Al-Muhtaseb, J. Kurdi, Emulsion stability and cross-linking of PMMA microcapsules containing phase change materials, *Sol. Energy Mater. Sol. Cells* 32 (2015) 311–318.
[22] P. Chaiyasat, S. Noppalit, M. Okubo, A. Chaiyasat, Do encapsulated heat storage materials really retain their original thermal properties? *Phys. Chem. Chem. Phys.* 17 (2015) 1053–1059.
[23] A. Sarı, C. Alkan, K. Karaipekli, Preparation, characterization and thermal properties of PMMA/*n*-heptadecane microcapsules as novel solid–liquid microPCM for thermal energy storage, *Appl. Energy* 87 (2010) 1529–1534.
[24] J. Huang, T.Y. Wang, P.P. Zhu, J.B. Xiao, Preparation, characterization, and thermal properties of the microencapsulation of a hydrated salt as phase change energy storage materials, *Thermochim. Acta* 557 (2013) 1–6.
[25] A. Sari, C. Alkan, A. Karaipekli, O. Uzun, Microencapsulated n-octacosane as phase change material for thermal energy storage, *Sol. Energy* 93 (2009) 1757–1763.
[26] C. Alkan, A. Sari, A. Karaipekli, O. Uzun, Preparation, characterization and thermal properties of microencapsulated phase change material for thermal energy storage, *Sol. Energy Mater. Sol. Cells* 93 (2009) 143–147.
[27] L. Wang, D. Meng, Fatty acid eutectic/polymethyl methacrylate composite as form-stable phase change material for thermal energy storage, *Appl. Energy* 87 (2010) 2660–2665.
[28] A.R. Shirin-Abadi, A.R. Mahdavian, S. Khoee, New approach for the elucidation of PCM nanocapsules through miniemulsion polymerization with an acrylic shell, *Macromolecules* 44 (2011) 7405–7414.
[29] Y. Wang, H. Shi, T.D. Xia, T. Zhang, H.X. Feng, Fabrication and performances of microencapsulated paraffin composites with polymethylmethacrylate shell based on ultraviolet irradiation-initiated, *Mater. Chem. Phys.* 135 (2012) 181–187.
[30] Y. Wang, Y. Zhang, T.D. Xia, W.J. Zhao, W.H. Yang, Effects of fabricated technology on particle size distribution and thermal properties of stearic–eicosanoic acid/polymethylmethacrylate nanocapsules, *Sol. Energy Mater. Sol. Cells* 120 (2014) 481–490.
[31] A. Chemtob, B. Kunstler, C. Croutxé-Barghorn, S. Fouchard, Photoinduced miniemulsion polymerization, *Colloid Polym. Sci.* 288 (2010) 579–587.
[32] M.Y. Wang, B.T. Tang, S.F. Zhang, Organic, cross-linking, and shape-stabilized solar thermal energy storage materials: A reversible phase transition driven by broadband visible light, *Appl. Energy* 113 (2014) 59–66.
[33] Y. Zuo, J. Hoigné, Photochemical decomposition of oxalic, glyoxalic and pyruvic acid catalysed by iron in atmospheric waters, *Atmos. Environ.* 28 (1994) 1231–1239.
[34] M.G. Neumann, C.C. Schmitt, I.C. Rigoli, The photoinitiation of MMA polymerization in the presence of iron complexes, *J. Photochem. Photobiol. A* 159 (2003) 145–150.
[35] X. Guo, A. Weiss, M. Ballauff, Synthesis of spherical polyelectrolyte brushes by photoemulsion polymerization, *Macromolecules* 32 (1999) 6043–6046.
[36] C.S. Chern, Y.C. Liou, Styrene miniemulsion polymerization initiated by 2, 2-azobisisobutyronitrile, *J. Polym. Sci. A* 37 (2000) 2537–2550.
[37] F. Wu, N.N. Deng, Photochemistry of hydrolytic iron (III) species and photoinduced degradation of organic compounds. A minireview, *Chemosphere* 41 (2000) 1137–1147.
[38] J. Giro-Paloma, M. Martínez, L.F. Cabeza, A.I. Fernández, Types, methods, techniques, and applications form icroencapsulated phase change materials (MPCM): A review, *Renew. Sust. Energ. Rev.* 53 (2016) 1059–1075.
[39] Y. Wang, H. Ji, H. Shi, T. Zhang, T.D. Xia, Fabrication and characterization of stearic acid/polyaniline composite with electrical conductivity as phase change materials for thermal energy storage, *Energy Convers. Manag.* 98 (2015) 322–330.
[40] J. Iqbal, Z. Ali, M. Hussain, R. Sheikh, K. Majeed, U. Khan, J. Ulrich, Formation of crystalline particles from phase change emulsion: Influence of different parameters, *Chin. J. Chem. Eng.* 24 (2016) 929–936.
[41] G. Alva, Y. Lin, L. Liu, G. Fang, Synthesis, characterization and applications of microencapsulatedphase change materials in thermal energy storage: A review, *Energy Build.* 144 (2017) 276–294.
[42] V. Kumar, B. Kandasubramanian, Processing and design methodologies for advanced and novel thermal barrier coatings for engineering applications, *Particuology* 27 (2016) 1–28.
[43] C. Jiao, B. Ji, D. Fang, Preparation and properties of lauric acid–stearic acid/expanded perlite composite as phase change materials for thermal energy storage, *Mater. Lett.* 67 (2012) 352–354.
[44] A. Karaipekli, A. Sari, Capric–myristic acid/vermiculite composite as form-stable phase change material for thermal energy storage, *Sol. Energy* 83 (2009) 323–332.
[45] A. Sari, C. Alkan, A.N. Özcan, Synthesis and characterization of micro/nano capsules of PMMA/capric–stearic acid eutectic mixture for low temperature-thermal energy storage in buildings, *Energy Build.* 90 (2015) 106–113.
[46] S.Y. Wu, D.S. Zhu, X.R. Zhang, J. Huang, Preparation and melting/freezing characteristics of Cu/paraffin nanofluid as phase-change material (PCM), *Energy Fuel* 24 (2010) 1894–1898.